

Article

Prediction, Application, and Mechanism Exploration of Liquid–Liquid Equilibrium Data in the Extraction of Aromatics Using Sulfolane

Shilong Dong ¹, Xiaoyan Sun ^{1,*}, Lili Wang ¹, Yanjing Li ¹, Wenying Zhao ², Li Xia ^{1,*} and Shuguang Xiang ¹

¹ Institute of Process System Engineering, College of Chemical Engineering, Qingdao University of Science and Technology, Qingdao 266042, China

² College of Chemistry and Chemical Engineering, Qilu Normal University, Jinan 250200, China

* Correspondence: sxy@qust.edu.cn (X.S.); xiali@qust.edu.cn (L.X.)

Abstract: Liquid–liquid equilibrium (LLE) data are critical for the design and optimization of processes for extracting aromatics. Partial LLE data for the non-aromatic–aromatic–sulfolane ternary system were acquired at 313.15 K and 101.3 kPa. The LLE data for the extraction of aromatics using sulfolane were predicted using the COSMO-RS model. Correspondingly, the predicted and experimental data were analyzed using the root mean square deviation (*RMSD*), distribution coefficient (*D*), and separation factor (*S*). The COSMO-RS model could better predict the LLE data for the extraction of aromatics by sulfolane. The results of quantum chemical calculation show that hydrogen bonds and van der Waals interactions between sulfolane–benzene and sulfolane–toluene were responsible for the strong selectivity of sulfolane for benzene and toluene over alkanes. The LLE data predicted by the COSMO-RS method using the UNIQUAC thermodynamic model were subjected to correlation analysis. The calculated *RMSD* values were all less than 0.0180, and the relative deviation (δ) between the simulated value of the main process index for the extraction column and the actual data was less than 2.5%, indicating that the obtained binary interaction parameters can be reliably used in designing and optimizing the extraction of aromatics using sulfolane.

Keywords: liquid–liquid equilibrium; aromatics extraction; quantum chemistry calculation; COSMO-RS model; UNIQUAC model



Citation: Dong, S.; Sun, X.; Wang, L.; Li, Y.; Zhao, W.; Xia, L.; Xiang, S. Prediction, Application, and Mechanism Exploration of Liquid–Liquid Equilibrium Data in the Extraction of Aromatics Using Sulfolane. *Processes* **2023**, *11*, 1228. <https://doi.org/10.3390/pr11041228>

Academic Editor: Li Xi

Received: 4 March 2023

Revised: 7 April 2023

Accepted: 11 April 2023

Published: 16 April 2023



Copyright: © 2023 by the authors. Licensee MDPI, Basel, Switzerland. This article is an open access article distributed under the terms and conditions of the Creative Commons Attribution (CC BY) license (<https://creativecommons.org/licenses/by/4.0/>).

1. Introduction

With the current emphasis on environmental protection and the rapid growth in the global demand for aromatics, green processes and large-scale production in the aromatics industry are required [1–4]. Aromatics is a general term that refers to hydrocarbons with a benzene ring structure in their molecules. The main sources of aromatics are cracked gasoline fractions and catalytic reformat oils. Trityl-benzene (benzene, toluene, and xylene, abbreviated as BTX), which is an important organic raw chemical material in the production of aromatics, can be used to fabricate synthetic fibers, resins, plastics, rubber, detergents, pharmaceuticals, and pesticides. The components of cracked gasoline fractions and catalytic reformat oils are extremely complex, and azeotropic systems are easily formed between different hydrocarbon substances and their isomers, such as alkanes, alkenes, cycloalkanes, and benzene; these azeotropes are difficult to separate via normal distillation [5,6]. For azeotropic hydrocarbon systems, separation is usually achieved industrially by extraction (liquid–liquid extraction) using sulfolane as the solvent.

Liquid–liquid equilibrium (LLE) data are critical for the extraction of aromatics. However, LLE data on the extraction of aromatics using sulfolane are not publicly available. Typically, experimental measurements are the most reliable way to obtain LLE data; however, in the design and optimization of aromatic extraction processes, it is impractical to obtain LLE data only through experiments. Compared with experimental measurements,

using theoretical predictions to obtain data on the LLE between different substances can conserve resources and provide a realistic guide for designing and developing processes [7].

Klamt et al. proposed a conductor-like screening model for real solvents (COSMO-RS) based on the conductor-like screening model (COSMO) [8–11]. In essence, the COSMO-RS model deals with solutes and solvents based on equivalent quantum chemistry and statistical thermodynamics, thus more accurately predicting the thermodynamic properties of the obtained substances. Based on the COSMO-RS model, Yang et al. [12] predicted the liquid–liquid equilibrium data for a system of polyoxymethylene dimethyl ethers, water, and extractants. Kang [13] predicted the ternary LLE data and mutual solubility of *n*-octanol, *n*-octanoic acid, and a solvent based on this method, and determined the best solvent for extracting naphthenic acid from diesel fuel. The COSMO-RS model has been successfully used to evaluate the thermodynamic parameters of ionic liquids [14–18] and deep eutectic solvents [19–24], where better results were expected. The COSMO-RS method does not require any experimental or physical data, and thermodynamic data such as LLE are directly obtained by quantum chemical and statistical thermodynamic predictions. Therefore, this model is a good choice for predicting the LLE parameters in the extraction of aromatics using sulfolane.

The mechanism of the extraction of aromatics using sulfolane was also previously explored based on quantum chemistry. In 2010, Johnson et al. [25] proposed a reduced density gradient (RDG) method, which can be used to study van der Waals interactions, hydrogen bonding, and spatial repulsion in systems. Similarly, the independent gradient model based on Hirshfeld partition (IGMH) has been used to study weak intermolecular and intramolecular interactions [26,27]. In contrast with the RDG method, the calculation in the IGMH method relies on the atomic coordinates, making this calculation fast, and the isosurface map plotted by this method is better than that of the RDG method. Moreover, the IGMH method can quantify the degree of influence of the interactions between different fragments, and can be colored with the help of visual molecular dynamics (VMD) [28] to achieve a more visual presentation. In addition to the aforementioned merits, the IGMH method has several advantages.

In this work, Section 2 provides partial experimental ternary LLE data, and other LLE data are obtained from references [29–31]. The methods and models used in this study are described in Section 3. In Section 4, the reliability of the experimental LLE data is validated. The LLE data for the extraction of aromatics using sulfolane are then analyzed using the COSMO-RS method, and the predicted and experimental data are discussed by considering the distribution coefficient (*D*) and separation factor (*S*). The σ -profiles of all substances in the studied process are explored. The mechanism of the extraction of aromatics using sulfolane is explored by analyzing the interaction energy and the type and intensity of the interactions in the different complexes. Finally, the predicted LLE data are correlated with the activity coefficient from the UNIQUAC model [32–35]. The relevant binary interaction parameters are also calculated and applied in the extraction of aromatics using sulfolane.

2. Experimental Details

2.1. Chemicals

In this work, the water content of sulfolane was determined using a Karl Fischer micro moisture analyzer. The water content (mass fraction) of sulfolane was less than 0.0271%, and the detailed analysis methods are provided in Supporting Information S1. Table S1 lists the details of the chemicals used in the experiment. In addition, all chemicals were directly used without any purification.

2.2. Equipment and Procedures

The LLE parameters were determined by using a liquid–liquid equilibrium kettle. Details of the experimental setup and procedural steps can be found in our previous work [36,37]. During the experiments, a pre-prepared mixture of sulfolane and two other reagents was added to the equilibrium kettle, stirred at a constant temperature for 2 h, and

statically layered for 4 h. Settling was to allow the system to reach a state of full equilibrium. The extract phase (lower layer) and raffinate phase (upper layer) liquids were carefully removed and the samples were analyzed by gas chromatography.

The specific test conditions for gas chromatography (Agilent GC7890A) are listed in Supporting Information Table S2. The initial temperature of the column was 343.15 K and held for 1 min, and then the temperature was increased to 503.15 K at a rate of 20 K·min⁻¹ and held for 10 min. The GC performance verification methods are described in Supporting Information S2 and Table S3. The quantitative correction factors for the different substances were calculated by analyzing standard solutions of known compositions. In this experiment, the experimental samples were processed by the external standard method, and measurements for each sample were performed at least in triplicate. The deviation of the three measurements was within ±0.1%.

3. Methods and Models

3.1. Entropy Analysis

The reliability of the tie line of the ternary LLE experimental data can be determined using the Hand [Equation (1)] and Othmer–Tobias [Equation (2)] empirical equations as follows [38,39]:

$$\ln \frac{x_2^{\text{II}}}{x_1^{\text{II}}} = a + b \ln \frac{x_2^{\text{I}}}{x_3^{\text{I}}} \quad (1)$$

$$\ln \left(\frac{1 - x_3^{\text{I}}}{x_3^{\text{I}}} \right) = c + d \ln \left(\frac{1 - x_1^{\text{II}}}{x_1^{\text{II}}} \right) \quad (2)$$

where x_2^{I} and x_3^{I} denote the molar fractions of aromatics and sulfolane in the extract phase and x_1^{II} and x_2^{II} represent the molar fractions of non-aromatics and aromatics in the raffinate phase, respectively. Additionally, a , b , c , and d are parameters in the Hand and Othmer–Tobias equations, respectively.

3.2. COSMO-RS Model

Klamt et al. applied quantum chemical calculations to a continuous medium solvation model and proposed COSMO theory. The thermodynamic properties of a substance were then predicted by calculating the σ -potential [8]. Klamt et al. proposed the COSMO-RS model [9–11]. The model describes the interaction between molecules as a pairwise fragment interaction, and combined with statistical thermodynamics, this model can be used to predict the phase equilibria and thermodynamic properties of multivariate systems. The calculation in the COSMO-RS model consists of two main steps: (1) Calculating molecular structures using quantum chemistry (QC) and obtaining the shielding charge density of the molecule ($p(\sigma)$), that is, the σ -profile. (2) Combining statistical thermodynamic methods to calculate the chemical potential ($\mu(\sigma)$).

3.3. Data Evaluation

The root mean square deviation (RMSD) was used to reflect the quality of the correlation between the LLE data and the calculated data, as shown in Equation (3).

$$RMSD = \left[\sum_{i=1}^3 \sum_{j=1}^2 \sum_{k=1}^n \frac{(x_{ijk}^{\text{pre}} - x_{ijk}^{\text{cal}})^2}{6n} \right]^{1/2} \quad (3)$$

here, i , j , and k represent the component, phase, and linkage, respectively; n represents the number of linkages; and x^{pre} and x^{cal} denote the predicted and calculated molar fractions, respectively.

3.4. DFT Calculation

The extraction mechanism of aromatics using sulfolane was explored by DFT calculation, and the geometric and interaction energies of the studied systems were calculated and analyzed using the quantum chemistry software Gaussian 09 [40]. Initial optimization of all substances was carried out at the ω B97X-D/6-31G(d, p) level, and optimization of the binary complexes was carried out at the ω B97X-D/6-311++G(d, p) level. The different conformations of the complexes were optimized on the basis of the lowest energy structure for geometric analysis and interaction energy ($\Delta E_{\text{interaction}}$) calculation [35,41,42]. The more negative the interaction energy, that is, the higher the value of $|\Delta E_{\text{interaction}}|$, the greater the gravitational force between the two molecules. Here, the interaction energy was obtained by correcting the calculation based on the basis set superposition error (BSSE) proposed by Boys and Bernardi [43].

$$\Delta E_{\text{interaction}} = E_{\text{AB}} - E_{\text{A}} - E_{\text{B}} + E_{\text{BSSE}} \quad (4)$$

$$E_{\text{BSSE}} = E_{\text{A}} - E_{(\text{A,AB})} + E_{\text{B}} - E_{(\text{B,AB})} \quad (5)$$

where E_{AB} is the energy of the AB complex under basis functions A and B. E_{A} is the energy of A under the A basis function, and E_{B} is the energy of B under the B basis function. E_{BSSE} represents the energy after the BSSE correction. $E_{(\text{A,AB})}$ represents the energy of A under the A and B basis functions, and $E_{(\text{B,AB})}$ represents the energy of B under the A and B basis functions.

The type and strength of the intermolecular interactions were analyzed using the RDG and IGMH methods. The weak interactions between different complexes were visualized using Multiwfn software [27,44,45], which is freely available online.

4. Results and Discussion

4.1. Reliability of Experimental LLE Data

Partial LLE equilibrium data were acquired for the non-aromatics (1)–aromatics (2)–sulfolane (3) ternary system at 313.15 K under a pressure of 101.3 kPa. The experimental conditions were determined according to the industrial feed situations. All the experimental data are presented in detail in Table 1. Additionally, the definition of partition coefficient (D) and separation factor (S) are shown in Supporting Information S3. In this work, the standard uncertainties were calculated based on Equation (6), and the standard uncertainties of compositions are shown in Table 2 [46]. The ternary LLE data of (cyclopentane/3-methylpentane)–aromatic–sulfolane were obtained at 313.15 K under a pressure of 101.3 kPa, and the missing parameters of cyclopentane and 3-methylpentane were added in the extraction of aromatics process using sulfolane. The experimental ternary phase diagrams are shown in Figures 1 and 2.

$$u = \sqrt{\frac{1}{N(N-1)} \sum_{i=1}^N (x_i - \bar{x}_i)^2} \quad (6)$$

where \bar{x}_i is the average value, x_i is mole fraction for composition i , and N is the number of experimental data.

Table 1. Liquid–liquid equilibrium data (molar fraction) for non-aromatics (1)–aromatics (2)–sulfolane (3) ternary systems at 313.15 K under 101.3 kPa ¹.

T/K	Sulfolane Rich Phase			Sulfolane Poor Phase			D	S
	x_1^I	x_2^I	x_3^I	x_1^{II}	x_2^{II}	x_3^{II}		
313.15	Cyclopentane (1)–Benzene (2)–Sulfolane (3)							
	0.0899	0.0000	0.9101	0.9990	0.0000	0.0010	–	–
	0.0841	0.1028	0.8131	0.9116	0.0856	0.0028	0.7633	13.0200
	0.1103	0.1770	0.7127	0.8557	0.1420	0.0023	0.8293	9.6635
	0.1051	0.2649	0.6300	0.7793	0.2159	0.0049	0.8522	9.0977
	0.1234	0.3127	0.5638	0.7344	0.2597	0.0059	0.8656	7.1641
	0.1385	0.3647	0.4968	0.6849	0.3101	0.0050	0.8751	5.8155
0.1380	0.4076	0.4544	0.6360	0.3524	0.0116	0.8845	5.3287	
313.15	3-Methylpentane (1)–Benzene (2)–Sulfolane (3)							
	0.0218	0.0000	0.9782	0.9886	0.0000	0.0114	–	–
	0.0282	0.0704	0.9014	0.8872	0.1101	0.0027	0.4696	20.13
	0.0388	0.1476	0.8136	0.7891	0.2010	0.0099	0.5532	14.94
	0.0450	0.2118	0.7432	0.7015	0.2884	0.0100	0.5631	11.44
	0.0488	0.2633	0.6879	0.6316	0.3607	0.0076	0.5672	9.45
	0.0786	0.4098	0.5116	0.4614	0.4844	0.0541	0.7094	4.97
0.0824	0.4444	0.4732	0.3833	0.5383	0.0784	0.7068	3.84	
313.15	Cyclopentane (1)–Toluene (2)–Sulfolane (3)							
	0.0726	0.0000	0.9274	0.9856	0.0000	0.0144	–	–
	0.0727	0.0444	0.8829	0.8791	0.0998	0.0211	0.2834	5.39
	0.0890	0.1586	0.7524	0.6929	0.2711	0.0360	0.4094	4.55
	0.1060	0.1986	0.6954	0.6122	0.3461	0.0417	0.4190	3.31
	0.1184	0.2197	0.6619	0.5735	0.3745	0.0521	0.4395	2.84
	0.1364	0.2582	0.6054	0.4806	0.4459	0.0735	0.4562	2.04
0.1437	0.3327	0.5236	0.3870	0.4860	0.1270	0.5758	1.84	
313.15	3-Methylpentane (1)–Toluene (2)–Sulfolane (3)							
	0.0229	0.0000	0.9771	0.9742	0.0000	0.0258	–	–
	0.0304	0.0828	0.8868	0.7879	0.1756	0.0366	0.3570	12.23
	0.0326	0.1253	0.8421	0.7077	0.2432	0.0492	0.3980	11.18
	0.0409	0.1849	0.7742	0.5770	0.3591	0.0638	0.4101	7.27
	0.0451	0.2268	0.7281	0.5176	0.4140	0.0684	0.4437	6.29
	0.0448	0.3066	0.6486	0.3953	0.5081	0.0966	0.5070	5.32
	0.0716	0.4218	0.5067	0.2865	0.6085	0.1050	0.6110	2.77
0.0719	0.4447	0.4834	0.2652	0.6158	0.1190	0.6442	2.67	

¹ Standard uncertainties (u) are $u(T) = 0.1$ K, $u(P) = 1$ kPa, and the standard uncertainties of compositions are listed in Table 2.

Table 2. The standard uncertainties of compositions for non-aromatics (1)–aromatics (2)–sulfolane (3) ternary systems at 313.15 K under 101.3 kPa.

T/K	Sulfolane Rich Phase			Sulfolane Poor Phase		
	$u(x_1^I)$	$u(x_2^I)$	$u(x_3^I)$	$u(x_1^{II})$	$u(x_2^{II})$	$u(x_3^{II})$
313.15	Cyclopentane (1)–Benzene (2)–Sulfolane (3)					
	0.0082	0.0555	0.0632	0.0488	0.0477	0.0013
313.15	3-Methylpentane (1)–Benzene (2)–Sulfolane (3)					
	0.0088	0.0626	0.0713	0.0828	0.0738	0.0111
313.15	Cyclopentane (1)–Toluene (2)–Sulfolane (3)					
	0.0109	0.0443	0.0548	0.0804	0.0679	0.0145
313.15	3-Methylpentane (1)–Toluene (2)–Sulfolane (3)					
	0.0064	0.0561	0.0623	0.0882	0.0767	0.0119

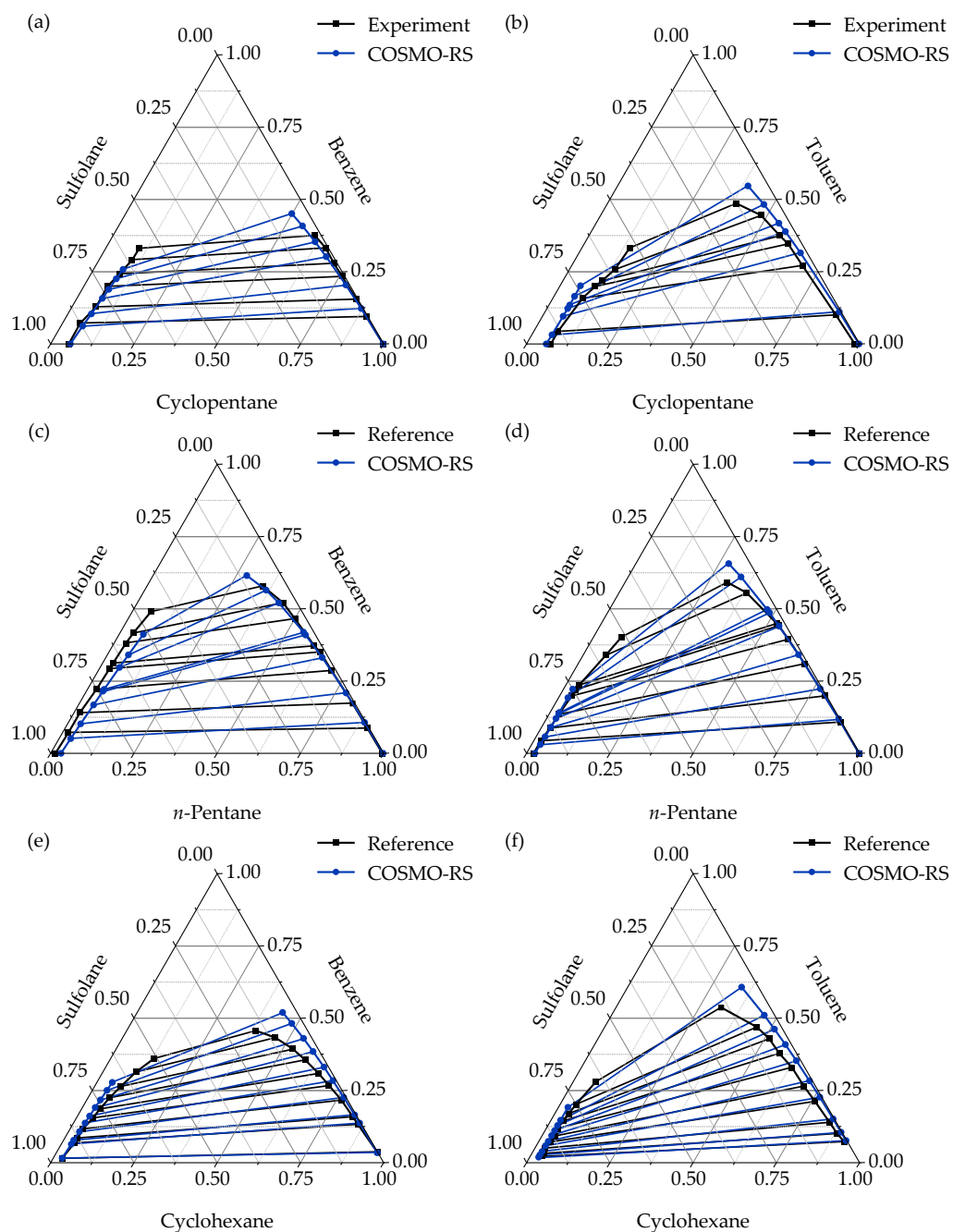


Figure 1. Ternary LLE data for (a) cyclopentane (1)–benzene (2)–sulfolane (3), (b) cyclopentane (1)–toluene (2)–sulfolane (3) at 313.15 K and 101.3 kPa, and ternary LLE data for (c) *n*-pentane (1)–benzene (2)–sulfolane (3) systems, (d) *n*-pentane (1)–toluene (2)–sulfolane (3), (e) cyclohexane (1)–benzene (2)–sulfolane (3), and (f) cyclohexane (1)–toluene (2)–sulfolane (3) at 298.15 K and 101.3 kPa. (■) Experimental or reference [29,30] data; (●) calculated data using the COSMO-RS model. (The method of Roozeboom was used to depict the composition of the ternary phase diagram).

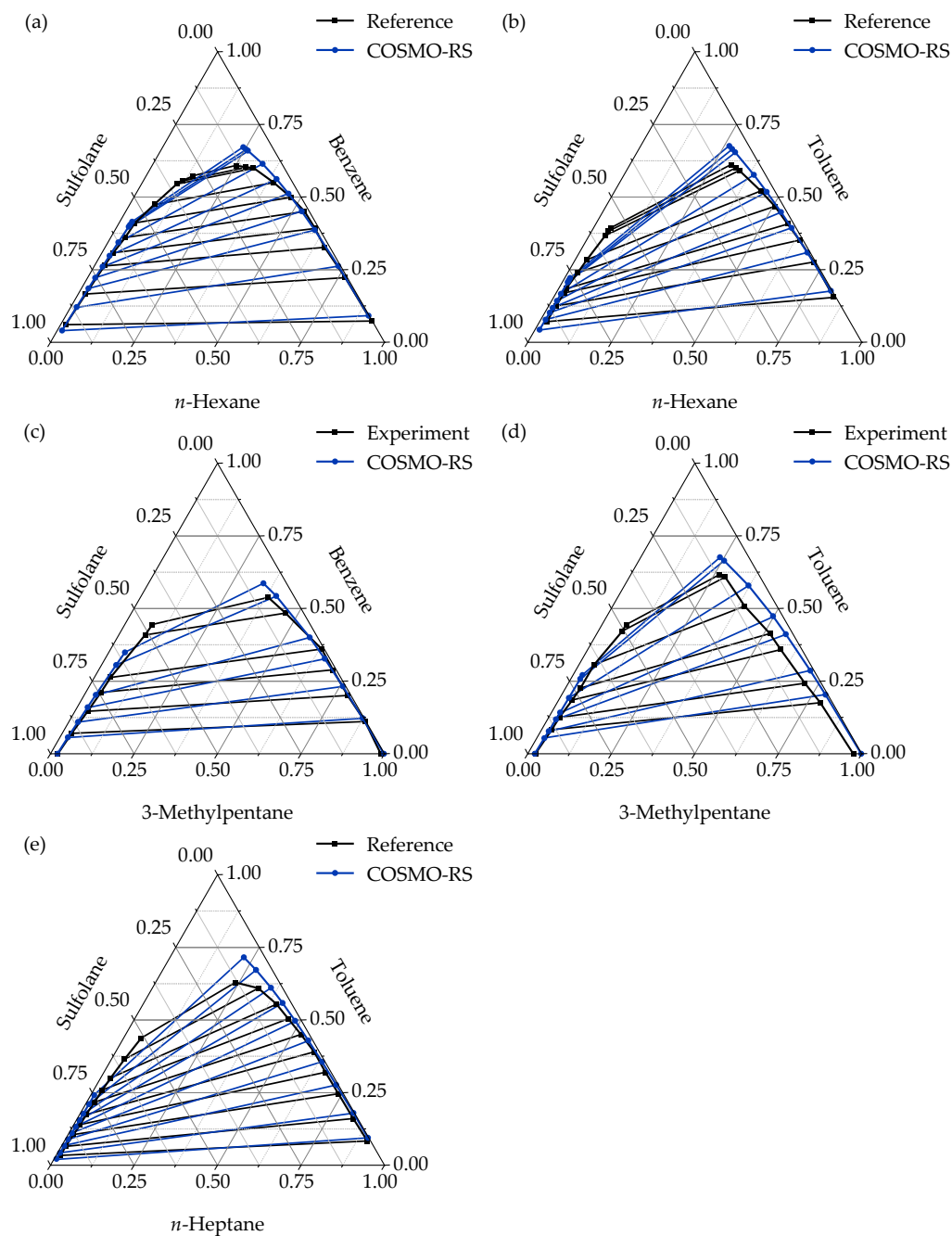
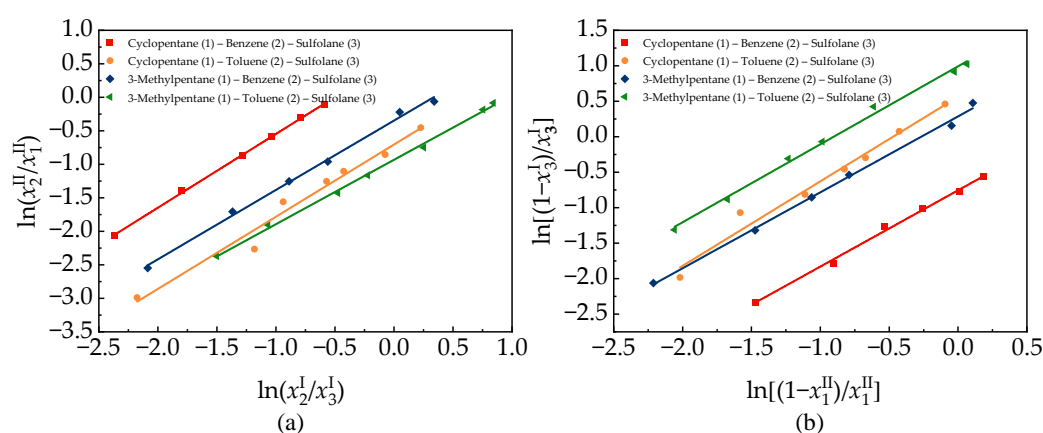


Figure 2. Ternary LLE data for (a) *n*-hexane (1)–benzene (2)–sulfolane (3), (b) *n*-hexane (1)–toluene (2)–sulfolane (3) systems at 298.15 K and 101.3 kPa, and ternary LLE data for (c) 3-methylpentane (1)–benzene (2)–sulfolane (3) and (d) 3-methylpentane (1)–toluene (2)–sulfolane (3) systems at 313.15 K and 101.3 kPa, and ternary LLE data for (e) *n*-pentane (1)–toluene (2)–sulfolane (3) system at 298.15 K and 101.3 kPa. (■) References [30,31] or experimental data; (●) calculated data using the COSMO-RS model. (The method of Roozeboom was used to depict the composition of the ternary phase diagram).

Table 3 shows the parameters a , b , c , and d for the Hand and Othmer–Tobias equations and the correlation coefficients R^2 for the different LLE data. Figure 3 shows the correlation fitting curves for these two equations. The R^2 for both equations were close to unity, indicating the high degree of consistency with the experimental data.

Table 3. The parameters of Hand and Othmer–Tobias equations for ternary LLE data under experimental conditions.

T/K	Hand			Othmer–Tobias		
	<i>a</i>	<i>b</i>	<i>R</i> ²	<i>c</i>	<i>d</i>	<i>R</i> ²
313.15	0.5543	1.1008	0.9994	−0.7549	1.0754	0.9963
313.15	−0.7047	1.0775	0.9729	0.5626	1.1913	0.9764
313.15	−0.3472	1.0352	0.9963	0.2863	1.0701	0.9968
313.15	−0.9323	0.9609	0.9975	0.9926	1.0990	0.9953

**Figure 3.** The correlation fitting curves for Hand and Othmer–Tobias equations. (a) Hand equation; (b) Othmer–Tobias equation.

4.2. Quantum Chemistry Computation and Analysis

4.2.1. COSMO-RS Calculation

The COSMO-RS model was developed using the COSMOthermX software (version 2020). Fortunately, the σ -profiles of benzene, toluene, sulfolane, cyclopentane, *n*-pentane, cyclohexane, *n*-hexane, 3-methylpentane, *n*-heptane, and 1-octene were obtained from the TZVPD-FINE database. The details of LLE data predicted using COSMO-RS are described in Supporting Information S4. Additionally, the LLE data predicted are presented in detail in Supporting Information Tables S4 and S5. Additionally, the ternary LLE phase diagrams predicted using COSMO-RS are shown in Figures 1 and 2. As shown in Supporting Information Table S6, the *RMSD* values were calculated to evaluate the COSMO-RS model. The calculated *RMSD* values range were between 0.0334 and 0.0898, indicating that the COSMO-RS model can better predict the LLE data for the extraction of aromatics using sulfolane. On the one hand, the data from references [29–31] with the predicted data using the COSMO-RS model were compared at 298.15 K under a pressure of 101.3 kPa, which proves the accuracy of the predicted results. On the other hand, considering the feed situations of the extraction operation, the experimental and predicted data were added at 313.15 K under a pressure of 101.3 kPa. To verify the effect of this part of the data on the modeling, the data for modeling was used and the simulation results showed its accuracy was good. The detailed instructions are provided in Supporting Information S5 and Table S7. As shown in Figures 4 and 5, on the other hand, the *D* values of benzene and toluene from the LLE data obtained using the COSMO-RS model prediction were lower than those obtained by experiment or from reference calculations, which may be due to the effect of hydrogen bonds between the aromatic hydrocarbons and sulfolane complexes. The *S* values of benzene and toluene obtained by prediction and experimental or reference

calculations were greater than one, indicating that the predicted separation of aromatic and non-aromatic compounds based on the COSMO-RS model is reliable.

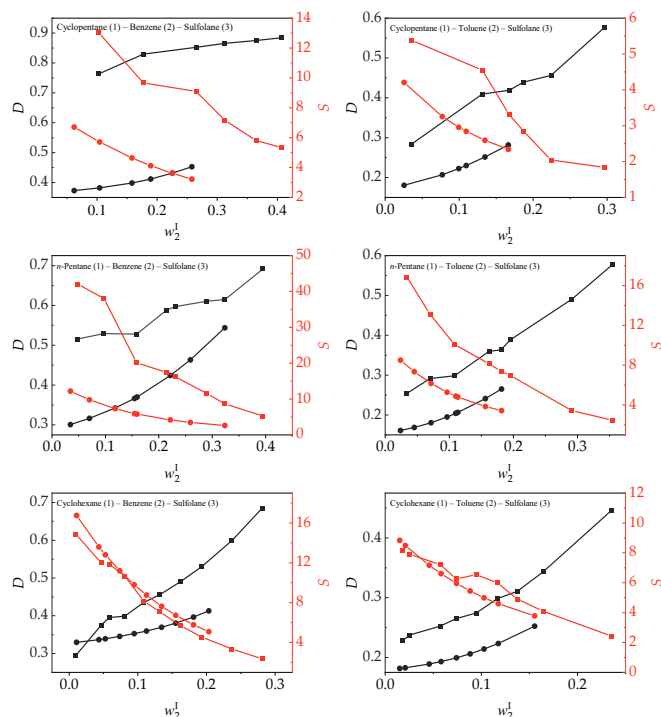


Figure 4. The distribution coefficients (D) and separation factors (S) of benzene and toluene (mass fraction) in the extracted phase (I). (■) Experimental or reference [29–31] data; (●) calculated data using the COSMO-RS model.

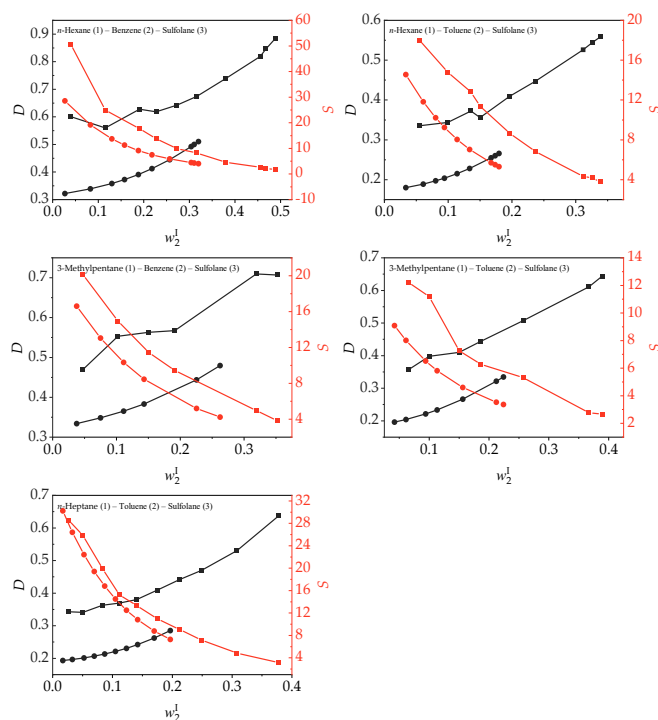


Figure 5. The distribution coefficients (D) and separation factors (S) of benzene and toluene (mass fraction) in the extracted phase (II). (■) Experimental or reference [30] data; (●) calculated data using the COSMO-RS model.

In summary, the predicted results accurately reflected the general trend of the experimental data. The predictions were in good agreement with the experimental or reference [29–31] results when the benzene or toluene concentration was low. In contrast, the COSMO-RS model predicted the extraction ability of sulfolane conservatively when benzene or toluene was present at a higher concentration. From an overall perspective, the data predicted by the COSMO-RS model were in good agreement with the data for the raffinate phase, but there was some error between the experimental and predicted values for the extract phase. Considering the fact that the COSMO-RS model is a prior model that does not require experimental data, and the difficulty of measuring LLE data experimentally, the COSMO-RS model is a good choice for initial simulation and prediction.

4.2.2. Interaction Analysis

From the σ -profile analysis of Supporting Information S6 and Figure S1, which explain the higher solubility of sulfolane in benzene and toluene, and according to the analysis results of Supporting Information S7, Table S8, and Figure S2, it is clear that sulfolane is more selective for benzene and toluene than alkanes.

In this study, extractant–aromatics and extractant–non-aromatics interactions represented by four complexes (sulfolane–benzene, sulfolane–toluene, sulfolane–cyclopentane, and sulfolane–*n*-hexane) were analyzed using RDG and IGMH. Figure 6a–d on the left shows the relationship between RDG and $\text{sign}(\lambda_2)\rho(\text{a.u.})$, where the right panel of Figure 6a–d shows the IGMH. Additionally, the RDG and IGMH of other complexes is shown as follows in Supporting Information Figure S3. The colors represent the different values of $\text{sign}(\lambda_2)\rho(\text{a.u.})$; the corresponding interaction types are shown in Figure 6e. In Figure 6e, the blue region with $\text{sign}(\lambda_2)\rho(\text{a.u.}) < 0$ is the region of strong interactions, such as hydrogen-bond interactions. The green region with the $\text{sign}(\lambda_2)\rho(\text{a.u.}) \approx 0$ indicates weak van der Waals interactions. If ring and cage structures are present in the molecule, strong mutual repulsive interactions are operative when $\text{sign}(\lambda_2)\rho(\text{a.u.}) > 0$, corresponding to the red region in the figure.

In the left panel of Figures 6a–d and S3a–d, a clear peak appears near the region where $\text{sign}(\lambda_2)\rho(\text{a.u.}) \approx 0.00$ for all four complexes, and a large green region is shown in the right panel, indicating the existence of weak van der Waals interactions between sulfolane–aromatics and sulfolane–non-aromatics. In addition, for sulfolane–toluene, the green region near $\text{sign}(\lambda_2)\rho(\text{a.u.}) \approx 0.00$, which indicates a weak interaction between sulfolane and toluene, is stronger than that of the other seven complexes. As shown in the isosurface plot, the hydrogen bonding interactions between the oxygen atom in sulfolane and the hydrogen atom in benzene (Figure 6a) and between the oxygen atom in sulfolane and the hydrogen atom of the methyl group in toluene (Figure 6b) were stronger than those of the other six complexes. Again, this difference can be clearly observed in the denseness of the blue region in the RDG diagram on the left side of Figures 6 and S3 (in the diagram, the blue regions for sulfolane–benzene and sulfolane–toluene are more dense than those of sulfolane–cyclopentane, sulfolane–*n*-hexane, sulfolane–*n*-pentane, sulfolane–cyclohexane, sulfolane–3-methylpentane, and sulfolane–*n*-heptane). The hydrogen atoms on the sulfolane ring and the π -bonds at the center of the aromatic ring form C–H $\cdots\pi$ bonds (weak hydrogen bonds), which is the green conical equivalent surfaces with larger areas on the right side of Figure 6a,b. The above analysis explains why the selectivity of sulfolane for benzene and toluene is stronger than that for the other investigated substances, which is consistent with the previous discussion of the interaction energy.

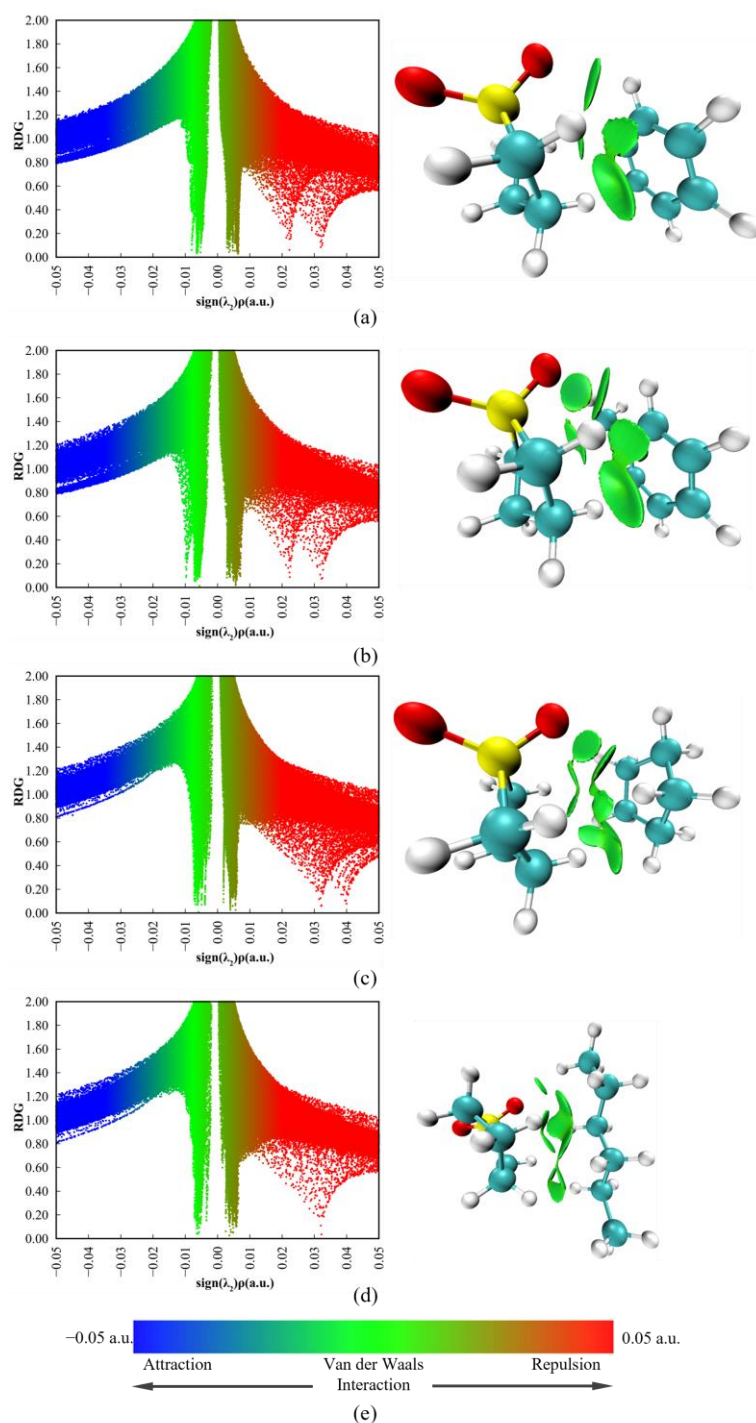


Figure 6. The RDG (left) and IGMH (right) of different complexes. (a) Sulfolane–Benzene; (b) Sulfolane–Toluene; (c) Sulfolane–Cyclopentane; (d) Sulfolane–*n*-Hexane; (e) The colors represented by the different $\text{sign}(\lambda_2)\rho$ (a.u.) values and the types of their corresponding interactions. (IGMH isovalue = 0.006).

4.3. Data Correlation

In this work, the LLE data predicted by the COSMO-RS model were correlated using the NRTL and UNIQUAC activity coefficient models. The calculation details of the NRTL and UNIQUAC models are presented in Supporting Information S8. The *RMSD* values are listed in Supporting Information Table S9. As can be seen from Table S9, the data correlated by the UNIQUAC model are more suitable for the extraction of aromatics. In

addition, it extends the support of the COSMO-RS method in thermodynamic modeling to the extraction of aromatics using sulfolane.

The binary interaction parameters and *RMSD* values are listed in Supporting Information Table S10. The calculated *RMSD* values were all less than 0.0180, where the UNIQUAC activity coefficient model indicated good correlation of the LLE data predicted by the COSMO-RS method.

4.4. Process Application and Analysis

In this section, the binary interaction parameters obtained from the regression analysis of the LLE data predicted by the COSMO-RS method are applied to the extraction of aromatics. The process was performed using an aromatics extraction device from a branch of SinoPec. A schematic of this process is shown in Figure 7. The columns in the aromatics extraction process include the extraction column (C01), raffinate oil washing column (C02), stripping column (C03), recovery column (C04), water stripping column (C05), and benzene column (C06). The feed compositions (stream two) of the extraction device are presented in Supporting Information Table S11, and the key component settings of the C01 are shown in Supporting Information Table S12. The relevant parameter settings for the column equipment are listed in Table 4. The aromatics extraction process utilizes sulfolane and aqueous polar components, and the whole system has strong non-ideality; thus, the UNIQUAC activity coefficient model was used for the global settings.

Table 4. Tower equipment parameters.

Equipment Name	Number of Theoretical Plates	Tower Pressure Drop/kPa	Tower Top Pressure/MPag
C01	33	280.00	0.52
C02	7	/	0.26
C03	34	49.25	0.10
C04	34	25.88	−0.05
C05	5	5.00	0.05
C06	60	53.00	0.05

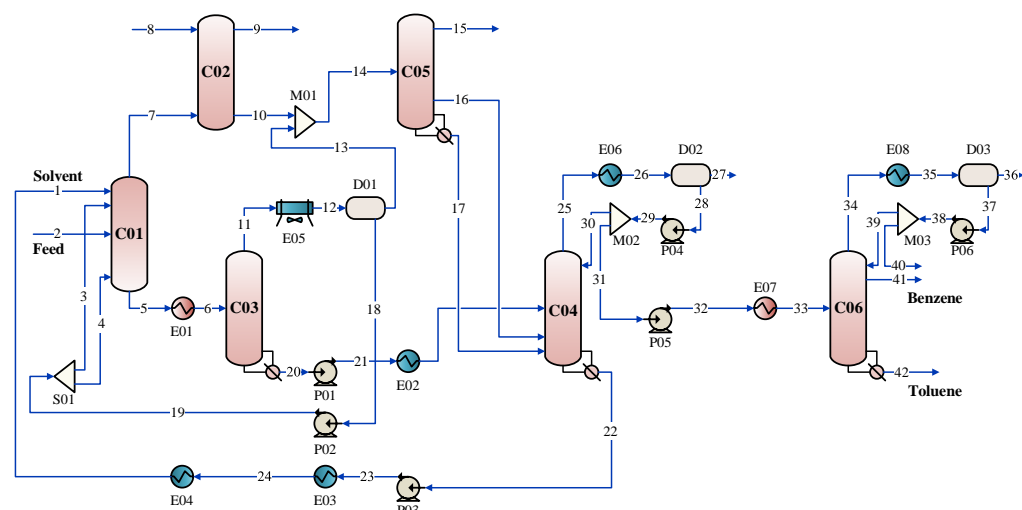


Figure 7. Schematic diagram of the process.

A full-process simulation was performed for the aromatics extraction process, where the mass fraction of the final benzene product was 99.96%, which meets the industrial requirements (mass fraction $\geq 99.8\%$). The simulation data for the key extraction equipment (extraction tower, C01) were analyzed and compared with the actual industrial data, provided that the final product met the industrial requirements. The absolute error (Δ)

was used to represent the difference between the simulated and measured values, and the relative error (δ) was used to measure the degree of deviation of the simulated values from the actual values. The equations for the calculation are as follows:

$$\Delta = x^{\text{sim}} - x^{\text{act}} \quad (7)$$

$$\delta = \frac{|x^{\text{sim}} - x^{\text{act}}|}{x^{\text{act}}} \quad (8)$$

where x^{sim} denotes the simulated values and x^{act} denotes the actual industrial data (the values of x^{act} are the actual laboratory analysis results of a SinoPec factory, Luoyang, China). A comparison of the main process indicators for C01 is presented in Table 5. Table 6 presents a comparison between the simulated results for the key components at the top and bottom of the C01 column and the actual industrial data.

Table 5. Comparison of main process indexes of C01.

Analysis Index	x^{act}	x^{sim}	Δ	$\delta\%$
Top pressure/MPag	0.52	0.52	0.00	0.00
Top temperature/K	360.30	360.77	0.47	0.54
Bottom temperature/K	336.83	335.98	−0.85	1.33

As can be seen from Table 5, in the simulated data for C01, the temperature at the top of the column is 0.47 K higher than the actual temperature, and the temperature at the bottom of the column is 0.85 K lower than the actual temperature. The overall absolute value of deviation was less than 1.33%, which is in line with the process index of the extraction column.

In Table 6, the deviation of the top key components and the bottom key components from the actual data was less than 2.5%. In summary, the binary parameters obtained from the LLE data predicted by the COSMO-RS model can be applied to the extraction of aromatics process using sulfolane.

Table 6. Comparison of main process indexes of C01.

	Components	x^{act} (Mass Fraction)	x^{sim} (Mass Fraction)	Δ	$\delta\%$
Column top	<i>n</i> -Pentane	9.72	9.74	0.02	0.21
	Cyclopentane	1.68	1.69	0.01	0.60
	<i>n</i> -Hexane	20.26	20.51	0.25	1.23
	Cyclohexane	1.22	1.23	0.01	0.43
	3-Methylpentane	26.07	26.07	0.00	0.00
	<i>n</i> -Heptane	12.51	12.82	0.31	2.46
Column bottom	Benzene	9.51	9.32	−0.19	2.00
	Toluene	16.49	16.18	−0.31	1.88
	Sulfolane	70.49	70.49	0.00	0.00

5. Conclusions

The LLE data for the extraction of aromatics using sulfolane were obtained using the COSMO-RS model. The predicted data were used for the extraction of aromatics using sulfolane. To determine the predicted data, the experimental and literature data analyses were carried out. The mechanism for the extraction of aromatics using sulfolane was discussed using DFT calculations. The significant findings in this study are as follows.

(1) Under a pressure of 101.3 kPa, representative non-aromatic–aromatic–sulfolane ternary LLE data were determined at 313.15 K. Simultaneously, the experimental LLE data were examined using the Hand and Othmer–Tobias equations, where R^2 was close to unity, indicating the reliability of the experimental data. The predicted data and experimental and

literature data were analyzed using *RMSD*, *D*, and *S*. The results showed that the calculated *RMSD* values range were between 0.0334 and 0.0898; the *D* values for benzene and toluene in the LLE data predicted by the COSMO-RS model were low, and the *S* values for benzene and toluene obtained by prediction were greater than unity. Overall, the results predicted by the COSMO-RS model can adequately reflect the general trend of the experimental data, but there are some errors.

(2) The mechanism of the extracting of aromatics using sulfolane was discussed using DFT calculations. The $|\Delta E_{\text{interaction}}|$ for the interplay of benzene–sulfolane and toluene–sulfolane is 28.74 kJ·mol^{−1} and 35.73 kJ·mol^{−1}, respectively, where these values are higher than the $|\Delta E_{\text{interaction}}|$ for the interaction of non-aromatics and sulfolane, whereas RDG and IGMH analyses indicated that hydrogen bonding and van der Waals interactions between sulfolane–benzene and sulfolane–toluene account for the strong selectivity of sulfolane for benzene and toluene over alkanes.

(3) The UNIQUAC thermodynamic model was successfully used to correlate the LLE data predicted by the COSMO-RS method and obtain binary interaction parameters. The calculated *RMSD* values were all less than 0.0180, and the deviation between the simulated value for the main process index of the extraction tower and the actual data were less than 2.5%, indicating that the obtained binary interaction parameters can be reliably used to design and optimize the extraction of aromatics using sulfolane.

The LLE data predicted by COSMO-RS can be used for the extraction of aromatics; it can serve as a theoretical reference for industrial application, and can also reduce the cost of investment.

Supplementary Materials: The following supporting information can be downloaded at: <https://www.mdpi.com/article/10.3390/pr11041228/s1>, S1. The detailed analysis method of water content in sulfolane; S2. The GC performance verification method. S3. The definition of partition coefficient (*D*) and separation factor (*S*); S4. The details of LLE data predicted using the COSMO-RS method; S5. The effect of feed situations on the extraction model; S6. The analysis of σ -profiles; S7. The interaction analysis; S8. The calculation details of NRTL and UNIQUAC models; Table S1. Chemical properties of materials; Table S2. The specific test conditions for Agilent GC7890A; Table S3. The test results of gas chromatograph (FID) performance verification; Table S4. Liquid–liquid equilibrium data (molar fraction) for non-aromatics (1)–benzene (2)–sulfolane (3) ternary systems at 293.15 K, or 313.15 K under 101.3 kPa using the COSMO-RS model; Table S5. Liquid–liquid equilibrium data (molar fraction) for non-aromatics (1)–toluene (2)–sulfolane (3) ternary systems at 293.15 K, or 313.15 K under 101.3 kPa using the COSMO-RS model; Table S6. The *RMSD* values of the COSMO-RS model at 293.15 K, or 313.15 K under 101.3 kPa; Table S7. Comparison of the main process indexes of C01; Table S8. Interaction energy of eight complexes corrected using BSSE; Table S9. The *RMSD* values of NRTL and UNIQUAC models; Table S10. The binary interaction parameters for ternary mixtures using a UNIQUAC model; Table S11. The feed compositions (stream 2) of the extraction device; Table S12. The key components setting of C01; Figure S1. The σ -profiles of the nine substances in this study; Figure S2. The complex configurations with the lowest energies; Figure S3. The RDG (left) and IGMH (right) of different complexes.

Author Contributions: Investigation, visualization, and writing—original draft, S.D.; conceptualization and writing—review and editing, X.S.; validation, methodology, and supervision, L.W.; methodology and software, Y.L.; supervision and validation, W.Z.; methodology and writing—review and editing, L.X.; investigation and validation, S.X. All authors have read and agreed to the published version of the manuscript.

Funding: This work was supported by the National Natural Science Foundation of China (NO. 22178190) and the National Youth Natural Science Foundation of China (NO. 22008129).

Data Availability Statement: The data presented in this study are available from the corresponding author upon request.

Conflicts of Interest: The authors declare no conflict of interest.

References

1. Mallah, M.A.; Li, C.; Mallah, M.A.; Noreen, S.; Liu, Y.; Saeed, M.; Xi, H.; Ahmed, B.; Feng, F.; Mirjat, A.A.; et al. Polycyclic aromatic hydrocarbon and its effects on human health: An overview. *Chemosphere* **2022**, *296*, 133948. [CrossRef]
2. Xiang, S.; Wang, L.; Wang, Y.; Bi, R.; Xia, L.; Sun, X. Exploration of gradient energy-saving separation processes for ethylene glycol mixtures based on energy, exergy, environment, and economic analyses. *Sep. Purif. Technol.* **2021**, *279*, 119787. [CrossRef]
3. Shekaari, H.; Zafarani-Moattar, M.T.; Mohammadi, B. Effective extraction of benzene and thiophene by novel deep eutectic solvents from hexane/aromatic mixture at different temperatures. *Fluid Phase Equilibria* **2019**, *484*, 38–52. [CrossRef]
4. Petrochemicals Market Size, Share & Trends Analysis Report by Product (Ethylene, Propylene, Butadiene, Benzene, Xylene, Toluene, Methanol), by Region, and Segment Forecasts, 2022–2030. 2022. Available online: <https://www.grandviewresearch.com/industry-analysis/petrochemical-market> (accessed on 12 October 2022).
5. Ma, S.; Li, J.; Li, L.; Shang, X.; Liu, S.; Xue, C.; Sun, L. Liquid-liquid extraction of benzene and cyclohexane using sulfolane-based low transition temperature mixtures as solvents: Experiments and simulation. *Energy Fuels* **2018**, *32*, 8006–8015. [CrossRef]
6. Shekaari, H.; Zafarani-Moattar, M.T.; Mohammadi, B. Liquid-liquid equilibria and thermophysical properties of ternary mixtures {(benzene/thiophene) + hexane + deep eutectic solvents}. *Fluid Phase Equilibria* **2020**, *509*, 112455. [CrossRef]
7. Gubbins, K.E.; Quirke, N. Molecular simulation and industrial applications: Methods, examples and prospects. *Curr. Top. Mol. Simul.* **1996**, *1*, 1–69.
8. Klamt, A.; Schueuermann, G. COSMO: A new approach to dielectric screening in solvents with explicit expressions for the screening energy and its gradient. *J. Chem. Soc.* **1993**, *2*, 799–805. [CrossRef]
9. Klamt, A. Conductor-like screening model for real solvents: A new approach to the quantitative calculation of solvation phenomena. *J. Phys. Chem.* **1995**, *99*, 2224–2235. [CrossRef]
10. Klamt, A.; Jonas, V.; Buerger, T.; Lohrenz, J.C.W. Refinement and parametrization of COSMO-RS. *J. Phys. Chem. A* **1998**, *102*, 5074–5085. [CrossRef]
11. Klamt, A.; Eckert, F. COSMO-RS: A novel and efficient method for the a priori prediction of thermophysical data of liquids. *Fluid Phase Equilibria* **2000**, *172*, 43–72. [CrossRef]
12. Yang, Z.; Ren, C.; Jiang, S.; Xin, Y.; Hu, Y.; Liu, Z. Theoretical predictions of compatibility of polyoxymethylene dimethyl ethers with diesel fuels and diesel additives. *Fuel* **2022**, *307*, 121797. [CrossRef]
13. Kang, S.; Kang, J. Extraction of naphthenic acid from low-grade crude oil using diol compounds. *Fuel* **2020**, *275*, 117828. [CrossRef]
14. Sun, D.; Feng, H.; Feng, X.; Li, W.; Zhang, Z. Evaluation of COSMO-RS model for the LLE prediction of benzene plus cyclohexane plus ionic liquid system. *J. Chem. Thermodyn.* **2020**, *145*, 106032. [CrossRef]
15. Khan, A.S.; Ibrahim, T.H.; Rashid, Z.; Khamis, M.I.; Nancarrow, P.; Jabbar, N.A. COSMO-RS based screening of ionic liquids for extraction of phenolic compounds from aqueous media. *J. Mol. Liq.* **2021**, *328*, 115387. [CrossRef]
16. Chin Ting, H.; Warsi Khan, H.; Vijaya Bhaskar Reddy, A.; Goto, M.; Moniruzzaman, M. Extraction of salicylic acid from wastewater using ionic liquid-based green emulsion liquid membrane: COSMO-RS prediction and experimental verification. *J. Mol. Liq.* **2022**, *347*, 118280. [CrossRef]
17. Zhang, Y.; Zhang, Q.; Hua, X.; Lv, M.; Zhang, Z. COSMO-RS prediction, liquid-liquid equilibrium experiment and quantum chemistry calculation for the separation of n-butanol and n-heptane system using ionic liquids. *J. Chem. Thermodyn.* **2022**, *167*, 106719. [CrossRef]
18. Shimul, I.M.; Moshikur, R.M.; Minamihata, K.; Moniruzzaman, M.; Kamiya, N.; Goto, M. Amino acid ester based phenolic ionic liquids as a potential solvent for the bioactive compound luteolin: Synthesis, characterization, and food preservation activity. *J. Mol. Liq.* **2022**, *349*, 118103. [CrossRef]
19. Li, G.; Gui, C.; Zhu, R.; Lei, Z. Deep eutectic solvents for efficient capture of cyclohexane in volatile organic compounds: Thermodynamic and molecular mechanism. *AIChE J.* **2022**, *68*, e17535. [CrossRef]
20. Santhi, V.M.; Ramalingam, A.; Sreekala, D.J.; Malaiyarsan, V.; Ayyavu, C. Ammonium based deep eutectic solvents (DESs) on extraction of benzothiophene from iso-octane: Experiment and COSMO-RS model. *J. Dispers. Sci. Technol.* **2022**, *43*, 1778–1788. [CrossRef]
21. Mulyono, S.; Hizaddin, H.F.; Wazeer, I.; Alqusair, O.; Ali, E.; Ali Hashim, M.; Hadj-Kali, M.K. Liquid-liquid equilibria data for the separation of ethylbenzene/styrene mixtures using ammonium-based deep eutectic solvents. *J. Chem. Thermodyn.* **2019**, *135*, 296–304. [CrossRef]
22. Salleh, Z.; Wazeer, I.; Mulyono, S.; El-Blidi, L.; Hashim, M.A.; Hadj-Kali, M.K. Efficient removal of benzene from cyclohexane-benzene mixtures using deep eutectic solvents—COSMO-RS screening and experimental validation. *J. Chem. Thermodyn.* **2017**, *104*, 33–44. [CrossRef]
23. Zurob, E.; Cabezas, R.; Villarroel, E.; Rosas, N.; Merlet, G.; Quijada-Maldonado, E.; Romero, J.; Plaza, A. Design of natural deep eutectic solvents for the ultrasound-assisted extraction of hydroxytyrosol from olive leaves supported by COSMO-RS. *Sep. Purif. Technol.* **2020**, *248*, 117054. [CrossRef]
24. Rodriguez, N.R.; Gerlach, T.; Scheepers, D.; Kroon, M.C.; Smirnova, I. Experimental determination of the LLE data of systems consisting of {hexane + benzene + deep eutectic solvent} and prediction using the Conductor-like Screening Model for Real Solvents. *J. Chem. Thermodyn.* **2017**, *104*, 128–137. [CrossRef]
25. Johnson, E.R.; Keinan, S.; Mori-Sanchez, P.; Contreras-Garcia, J.; Cohen, A.J.; Yang, W. Revealing noncovalent interactions. *J. Am. Chem. Soc.* **2010**, *132*, 6498–6506. [CrossRef]

26. Lefebvre, C.; Rubez, G.; Khartabil, H.; Boisson, J.; Contreras-Garcia, J.; Henon, E. Accurately extracting the signature of intermolecular interactions present in the NCI plot of the reduced density gradient versus electron density. *Phys. Chem. Chem. Phys.* **2017**, *19*, 17928–17936. [CrossRef] [PubMed]
27. Lu, T.; Chen, Q. Independent gradient model based on Hirshfeld partition: A new method for visual study of interactions in chemical systems. *J. Comput. Chem.* **2022**, *43*, 539–555. [CrossRef]
28. Humphrey, W.; Dalke, A.; Schulten, K. VMD: Visual molecular dynamics. *J. Mol. Graph.* **1996**, *14*, 27–28, 33–38. [CrossRef]
29. Cassell, G.W.; Dural, N.; Hines, A.L. Liquid-liquid equilibrium of sulfolane–benzene–pentane and sulfolane–toluene–pentane. *Ind. Eng. Chem. Res.* **1989**, *28*, 1369–1374. [CrossRef]
30. Chen, J.; Li, Z.; Duan, L. Liquid-liquid equilibria of ternary and quaternary systems including cyclohexane, 1-heptene, benzene, toluene, and sulfolane at 298.15 K. *J. Chem. Eng. Data* **2000**, *45*, 689–692. [CrossRef]
31. Chen, J.; Duan, L.P.; Mi, J.G.; Fei, W.Y.; Li, Z.C. Liquid-liquid equilibria of multi-component systems including n-hexane, n-octane, benzene, toluene, xylene and sulfolane at 298.15 K and atmospheric pressure. *Fluid Phase Equilibria* **2000**, *173*, 109–119. [CrossRef]
32. Renon, H.; Prausnitz, J.M. Local compositions in thermodynamic excess functions for liquid mixtures. *AIChE J.* **1968**, *14*, 135–144. [CrossRef]
33. Abrams, D.S.; Prausnitz, J.M. Statistical thermodynamics of liquid mixtures. New expression for the excess Gibbs energy of partly or completely miscible systems. *AIChE J.* **1975**, *21*, 116–128. [CrossRef]
34. Wang, Z.; Fan, W.; Xu, D.; He, S.; Huang, H.; Gao, J.; Wang, Y. Liquid-liquid phase equilibrium for quaternary systems (n-decane + 1-tetradecene + 1-methylnaphthalene + sulfolane/dimethyl sulfoxide) for separation of 1-methylnaphthalene from FCC diesel. *J. Chem. Eng. Data* **2021**, *66*, 2803–2811. [CrossRef]
35. Li, H.; Zhang, Y.; Zhao, L.; Sun, D.; Gao, J.; Xu, C. Liquid-liquid equilibria and mechanism exploration for the extraction of sulfides from FCC naphtha via organic solvent as extractant. *J. Mol. Liq.* **2021**, *327*, 114821. [CrossRef]
36. Sun, X.; Xiang, S. Study on Liquid-liquid equilibrium of 2-methylbutane/2,2-dimethylbutane-benzene-sulfolane ternary systems. *J. Chem. Eng. Chin. Univ.* **2014**, *28*, 412–415. [CrossRef]
37. Sun, X.; Xiang, S. Liquid-liquid equilibria of ternary systems cis-1,2-dimethylcyclohexane + toluene + sulfolane. *Chin. J. Chem. Eng.* **2014**, *22*, 1298–1301. [CrossRef]
38. Hand, D.B. Dimeric distribution. *J. Phys. Chem.* **1930**, *34*, 1961–2000. [CrossRef]
39. Othmer, D.; Tobias, P. Liquid-liquid extraction data—The line correlation. *Ind. Eng. Chem.* **1942**, *34*, 693–696. [CrossRef]
40. Frisch, M.; Trucks, G.; Schlegel, H.; Scuseria, G.; Robb, M.; Cheeseman, J.; Scalmani, G.; Barone, V.; Mennucci, B.; Petersson, G. *Gaussian 09 (Revision D.01)*; Gaussian, Inc.: Wallingford, CT, USA, 2009.
41. Zhan, G.; Shen, B.; Sun, H.; Chen, X. Extractive distillation approach to the removal of dimethyl disulfide from methyl tert-butyl ether: Combined computational solvent screening and experimental process investigation. *Ind. Eng. Chem. Res.* **2018**, *57*, 3348–3358. [CrossRef]
42. Lu, T. Molclus Program, Version 1.9.9.6. Available online: <https://www.keinsci.com/research/molclus.html> (accessed on 24 November 2022).
43. Boys, S.F.; Bernardi, F. The calculation of small molecular interactions by the differences of separate total energies. Some procedures with reduced errors. *Mol. Phys.* **2002**, *19*, 553–566. [CrossRef]
44. Lu, T.; Chen, F. Multiwfn: A multifunctional wavefunction analyzer. *J. Comput. Chem.* **2012**, *33*, 580–592. [CrossRef] [PubMed]
45. Lu, T.; Chen, F. Quantitative analysis of molecular surface based on improved marching tetrahedra algorithm. *J. Mol. Graph. Modell.* **2012**, *38*, 314–323. [CrossRef] [PubMed]
46. Thidarat, W.; Milan, H.; Tomas, S.; Natchanun, L.; Ura, P.; Suphot, P. Ternary (liquid-liquid) equilibrium data of furfuryl alcohol with organic solvents at T = 298.2 K: Experimental results and thermodynamic models. *Fluid Phase Equilibria* **2014**, *365*, 88–96. [CrossRef]

Disclaimer/Publisher’s Note: The statements, opinions and data contained in all publications are solely those of the individual author(s) and contributor(s) and not of MDPI and/or the editor(s). MDPI and/or the editor(s) disclaim responsibility for any injury to people or property resulting from any ideas, methods, instructions or products referred to in the content.